https://doi.org/10.5194/egusphere-2025-6011
Preprint. Discussion started: 12 December 2025


# Symbolic regression-based regionalization of baseflow separation parameter using catchment-scale characteristics

Yongen Lin[1,2], Dagang Wang[1,2*], Yiwen Mei[2], Jinxin Zhu[1,2], Huan Wu[3,4], Shuo Wang[5], Zhonghou Xu[6], Asaad Y. Shamseldin[7], Emmanouil N. Anagnostou[8]

[1] School of Geography and Planning, Sun Yat-sen University, Guangzhou, China

[2] Carbon-Water Research Station in Karst Regions of Northern Guangdong, Sun Yat-sen University, Guangzhou, China

[3] School of Atmospheric Science, Sun Yat-sen University, Zhuhai, Guangdong, China

[4] State Key Laboratory of Climate System Prediction and Risk Management, Nanjing University of Information Science and Technology, Nanjing, China

[5] Department of Land Surveying and Geo-informatics, Hong Kong Polytechnic University, Kowloon, Hong Kong Special Administrative Region, China

[6] Earth Sciences New Zealand, Hamilton 3216, New Zealand

[7] Department of Civil and Environmental Engineering, The University of Auckland, Auckland 1010, New Zealand

[8] Department of Civil and Environmental Engineering, University of Connecticut, Storrs, USA

*Correspondence to*: Dagang Wang (wangdag@mail.sysu.edu.cn)

**Abstract.** Accurate separation of baseflow from streamflow is of utmost importance for understanding catchment hydrological processes and supporting effective water resource management. The Smooth Minima Method is a common baseflow separation technique with a segment length parameter ($N$) representing the catchment average flow event duration. $N$ is usually predicted by a power function with catchment area or default to 5 days. Yet these estimations are insufficient given the multivariate nature of $N$ with other catchment attributes. In this study, we employ symbolic regression (SR) to search for possible formulation of $N$ with a range of catchment attributes based on 855 catchments across the Contiguous United States. We ultimately identify three mathematical expressions of increasing complexity, achieving $R^2$ values of 0.49, 0.50, and 0.54, compared to 0.23 and -0.84 for the power function and constant values. The three expressions reveal that $N$ increases exponentially with catchment area ($A$) and catchment-averaged soil saturated hydraulic conductivity ($K_{sat}$) with decreasing rates, while it increases linearly with snow day fraction ($f_{SWE}$). The effects of $K_{sat}$ and $f_{SWE}$ on $N$ are particularly pronounced for larger values ($K_{sat} > 25$ mm/h and $f_{SWE} > 0.4$) and smaller area ($A < 100$ km$^2$). The different calculations of $N$ are also evaluated in baseflow separation, revealing higher medians of Kling-Gupta Efficiency of at least 0.84, outperforming the literature-suggested formulas for a maximum increment of 0.22. This study highlights the potential of SR for uncovering physically meaningful formulas in optimal baseflow separation.

https://doi.org/10.5194/egusphere-2025-6011
Preprint. Discussion started: 12 December 2025


## 1. Introduction

Baseflow is an essential component of streamflow, primarily originating from groundwater, deep interflow, snow melting, and other delayed sources (Stoelzle et al., 2020; Wang et al., 2022; Xie et al., 2020). The proportion of baseflow in streamflow reflects the complex interactions between surface water and groundwater systems (Pelletier and Andréassian, 2020; Xie et al., 2024), and understanding this proportion can aid in water resources management and riverine ecosystem conservation (Tan et al., 2020; Yan et al., 2023). Baseflow is difficult to measure directly and it is usually estimated using baseflow separation methods (Humphrey et al., 2022; Stewart, 2015), which take continuous streamflow data as the only inputs. The performance of baseflow separation is sensitive to parameters of the separation methods, which, if not optimized, may lead to unrealistic baseflow dynamics (Mei et al., 2024a). Incorporating environmental tracer data for parameter optimization is a common practice, as it ensures reliable baseflow separation by maintaining dual mass balance for both tracer concentration and streamflow volume (Cartwright, 2022; Hagedorn, 2020; McMahon and Nathan, 2021). However, a critical challenge arises as this method is not applicable for catchments without continuous tracer data, which unfortunately constitutes the majority of gaged catchments worldwide (Hou et al., 2024; Thorslund and van Vliet, 2020). This limitation hinders accurate quantification of baseflow in most global catchments, despite their long-term streamflow data.

To optimize baseflow separation for gaged catchment lacking continuous environmental tracer data, a viable approach is to transfer optimized parameters from other catchments (Feigl et al., 2020; Klotz et al., 2017). Specifically, prediction models can be developed for these optimized parameters based on factors representing catchment physical conditions. This approach is fundamentally rooted in the hydrological similarity theory, which assumes that baseflow parameters reflect the catchment's hydrological signatures and relate to its physical characteristics (Gnann et al., 2021; McMillan et al., 2022; Price, 2011; Zhang et al., 2020). While this parameter regionalization approach is widely used for transferring calibrated parameters to un-gaged catchments in hydrological modeling (Feigl et al., 2020; Klotz et al., 2017), its application in the context of baseflow parameters is unexplored. The smooth minima method (SMM) is a widely used method for baseflow separation, with a segment length parameter ($N$) representing the average streamflow delay and catchment response (Stoelzle et al., 2020). This parameter is often defaulted to 5 days or estimated by an empirical power-law relationship with drainage area ($A$) as $N = 1.6 \times A^{0.2}$ (Aksoy et al., 2008). However, Lin et al. (2025b) found that while $A$ is the most influential predictor, incorporating additional factors representing geomorphology, climate, soil hydraulics properties, and human activities into the nonparametric random forest (RF) model yielded more accurate estimates than the power function. This highlights the complex interactions between streamflow delay and the diverse catchment characteristics (Price, 2011; Stoelzle et al., 2020).

Despite higher prediction accuracy, the RF-based regionalization model remains a "black box" with no explicit expression linking catchment attributes to parameter $N$ (Rudin, 2019). Although partial dependence plots may be adopted to explore the functional relationships between catchment attributes and $N$, they cannot mathematically formulate these relationship (Makke and Chawla, 2024; Rudin, 2019). To develop interpretable regionalization models for the optimal baseflow parameters $N$, this study employs an emerging machine learning technique called symbolic regression (SR), which focuses on data-driven equation discovery (Koza, 1994; Song et al., 2024). Unlike a "black-box" model such as RF, SR derives explicit and concise equations that identify underlying data patterns, while

https://doi.org/10.5194/egusphere-2025-6011
Preprint. Discussion started: 12 December 2025


mitigating overfitting through complexity control (Kronberger et al., 2022; Wilstrup and Kasak, 2021). This enables direct interpretation of how catchment attributes govern baseflow parameter values, which in terms influence the partitioning of streamflow (Feigl et al., 2020; Klotz et al., 2017; Sheta et al., 2023).

To evaluate the effectiveness for regionalization of baseflow parameters, this study applies SR to model the segment length parameter of SMM and addresses three objectives: a) assess the complexity-performance trade-off of SR-derived formulas for $N$; b) explore the functional relationships between $N$ and catchment attributes in the SR formulas; and c) evaluate the different $N$s calculated by SR in baseflow separation. This study should not be viewed as an effort to assert a superior utility of SR over other machine learning models in the regionalization of baseflow parameters. Instead, the SR formulas serve as post-hoc interpretability tools to complement other black box models, enhancing transparency into the relationship between hydrological signatures and catchment attributes (Rudin, 2019).

## 2. Study catchments and data

This study used the baseflow dataset produced by Mei et al. (2024b), which contains the segment length parameter of SMM optimized by specific electrical conductance (SEC) for 987 catchments across the Continental United States (CONUS). To reduce uncertainty due to the limited suitability of SMM in certain catchments, those exhibiting suboptimal baseflow separation performance—operationalized as a Kling Gupta Efficiency between estimated and observed SEC below 0.5 (Mei et al., 2024b) – were excluded from the study. Additionally, catchments with incomplete attribute data (see the next paragraph for details) were also eliminated. After applying these criteria, a total of 855 catchments remained. The spatial distribution of these catchments, overlaid with drainage area, mean streamflow, and baseflow index (BFI), is depicted in **Figure 1**a-c, showing significant diversity. The optimal $N$ parameters for these catchments are depicted in **Figure 1**d with most values smaller than 17 days and no clear spatial patterns. The level 2 and level 4 Hydrological Unit Codes (HUC2 and HUC4), which represent large and sub-regional hydrologic basins in the United States, are provided for better referencing the spatial distributions of results in the analysis (**Figure 1**e, f).

https://doi.org/10.5194/egusphere-2025-6011
Preprint. Discussion started: 12 December 2025


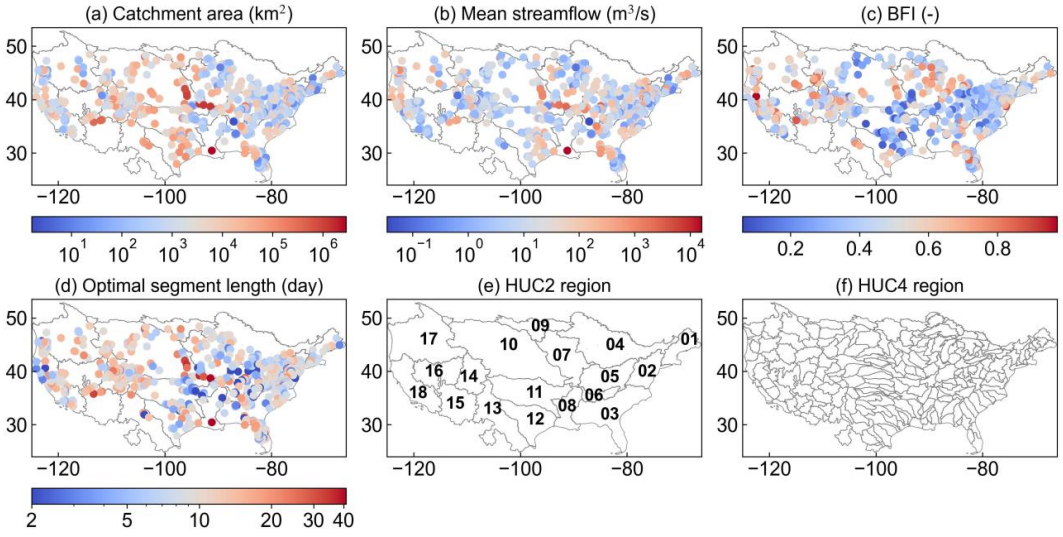


**Figure 1. Spatial distribution of the 855 selected catchments with their drainage area (a), mean streamflow (b), BFI (c), and optimal segment length parameter *N* (d) superimposed on HUC2 regions. The HUC2 and HUC4 region maps are provided for referencing (e, f).**

Lin et al. (2025b) revealed that 13 catchment characteristics representing the geomorphology, climate, soil hydraulic condition, and water usage are influential to the prediction of *N* (**Table 1**, rows 1-13). In addition to these 13 characteristics, we added two more related to snow processes and vegetation dynamics as inputs to SR (**Table 1**, rows 14-15). This is because some studies found that snow processes and vegetation dynamics can have nonnegligible impacts on baseflow generation (Price, 2011; Stoelzle et al., 2020; Xie et al., 2022). The Pearson correlation coefficients between these characteristics and the segment length parameter range from -0.45 to 0.53 (**Figure B1**).

https://doi.org/10.5194/egusphere-2025-6011
Preprint. Discussion started: 12 December 2025


**Table 1. Catchment characteristics used as inputs to the SR method for predicting parameter *N*.**

| | Name | Description (unit) | Data sources and calculation processes |
|---|---|---|---|
| 1 | $PE_x$ | Maximum daily potential evapotranspiration (mm/day) | Lin et al. (2025a) |
| 2 | $TX_x$ | Maximum daily maximum temperature (℃) | |
| 3 | $P_{95}$ | The 95-th percentile of daily precipitation larger than 0.01 mm (mm/day) | |
| 4 | $P_{50}$ | Median of daily precipitation larger than 0.01 mm (mm/day) | |
| 5 | $P_5$ | The 5-th percentile of daily precipitation larger than 0.01 mm (mm/day) | |
| 6 | $f_P$ | Proportion of days with precipitation larger than 0.01 mm (-) | |
| 7 | $f_{cly}$ | Volumetric fraction of clay (-) | |
| 8 | $W_{sat}$ | Saturated water capacity (%) | |
| 9 | $k_{sat}$ | Saturated hydraulic conductivity ($\times 10^{-2}$ mm/hour) | |
| 10 | $A$ | Catchment area (km$^2$) | |
| 11 | $R_E$ | Elongation ratio (-) | |
| 12 | $\bar{S}$ | Mean daily storage of reservoirs ($\times 10^6$ m$^3$) | |
| 13 | $S_{SD}$ | Standard deviation of daily storage of reservoirs ($\times 10^6$ m$^3$) | |
| 14 | $f_{SWE}$ | Proportion of days with snow water equivalent larger than 0.05 mm (-) | Snow Data Assimilation System, SNODAS (NOHRSC, 2004). $f_{SWE} = \frac{1}{\lvert D \rvert}\sum_{d\in D} I_d(SWE_d > 0.05)$ |
| 15 | $\overline{LAI}$ | Mean 16-daily leaf area index (-) | GLobal HYdrogeology MaPS of permeability and porosity (GLOBMAP) LAI v3 (Liu et al., 2012) |

**Quantities:**

$\boldsymbol{D}$: number of days in a year; $\boldsymbol{SWE_d}$: catchment-averaged snow water equivalent of day $d$; $\boldsymbol{I_d(SWE_d > 0.05)}$: an indicator showing that if $SWE_d$ is larger than 0.05 mm.

## 3. Methods

### 3.1. Recaps on Smooth Minima Baseflow Separation (SMM)

SMM is a widely used baseflow separation method (Aksoy et al., 2008; Piggott et al., 2005; Tan et al., 2020; Xie et al., 2020). It assumes that baseflow constitutes 100% of streamflow during low-flow periods (Gustard et al., 1992). The method involves two key parameters: the segment length parameter ($N$) and the filtering coefficient parameter ($M$). The segment length parameter $N$ is a proxy of the flow event duration (Stoelzle et al., 2020). Generally, a smaller $N$ result in a higher proportion of baseflow in streamflow, implying shorter surface flow duration. In the literature, $N$ is often default to 5 days or predicted using a power-law relationship with catchment area, namely $N = 1.6 \times A^{0.2}$, where $A$ is the catchment area in km$^2$ (Aksoy et al., 2008; Zhang et al., 2017). These two formulations of $N$ are included in the subsequent comparison and are denoted as $F_D$ and $F_{PL}$, respectively.

https://doi.org/10.5194/egusphere-2025-6011
Preprint. Discussion started: 12 December 2025


The filtering coefficient parameter *M* is used to determine if a streamflow minimum qualifies as a strict baseflow point. Higher values of *M* (typically not exceeding 1) correspond to more stringent criteria for identifying pure baseflow conditions. Unlike *N*, the parameter *M* is less sensitive to the baseflow separation results and is commonly assigned a constant value of 0.9 (Aksoy et al., 2008; Stoelzle et al., 2020).

### 3.2. Symbolic regression modelling for the segment length parameter

In this study, the symbolic regression (SR) is employed to derive expressions for the parameter *N*. SR represents an expression using a tree structure, where each node corresponds to a mathematical operator, and each leaf represents an input variable or constant. Structure of the tree evolves to identify expressions that best fit the inputted data through genetic programming (Koza, 1994). For example, **Figure 2**a illustrates five SR trees representing different expressions within the dotted box. The SR method is implemented using the PySR library in Python (Cranmer, 2023). The fifteen catchment characteristics (**Table 1**) are used as inputs. The mathematical operators for training the SR models includes input variables, constants, addition, subtraction, multiplication, division, exponential, and logarithmic operators. The SR method evaluates both accuracy and complexity of each candidate expression to select the most accurate formulation under different levels of complexity allowance. Expression complexity is defined as the sum of the complexity index assigned to each component in the equation. Take $N = 1.6 \times A^{0.2}$ as an example, if multiplication and exponential operators are each assigned a complexity of 2 and constants and input variables are assigned a complexity of 1, the total complexity of the expression is calculated as $2 + 2 + 1 + 1 + 1 = 7$. To train SR models, complexity index for each possible mathematical operator is set to 1 to avoid bias among the operators; the maximum allowable complexity for the resulting expressions is set to 20. The goodness of fit between the reference and the predicted *N*s is evaluated using the mean squared error ($MSE$):

$$MSE = \frac{1}{C}\sum_{i=1}^{C}\left(N_i - \hat{N}_i\right)^2 \quad , \qquad (1)$$

where $C$ is the total number of catchments, and $N_i$ and $\hat{N}_i$ represent the reference and predicted values of *N* for catchment $i$, respectively.

To evaluate the robustness of the SR models, a ten-fold cross-validation strategy is employed (**Figure 2**a). The 855 catchments are randomly partitioned into ten subsets of approximately equal size. In each iteration, the model is trained on nine subsets and tested on the remaining one to estimate the generalization error. This process is repeated ten times so that each subset serves once as the testing set. In each iteration, 7 to 10 expressions with varying levels of complexity are generated, resulting in a total of 91 expressions. Among these expressions, we identified recurrent equation forms across all ten iterations.

https://doi.org/10.5194/egusphere-2025-6011
Preprint. Discussion started: 12 December 2025


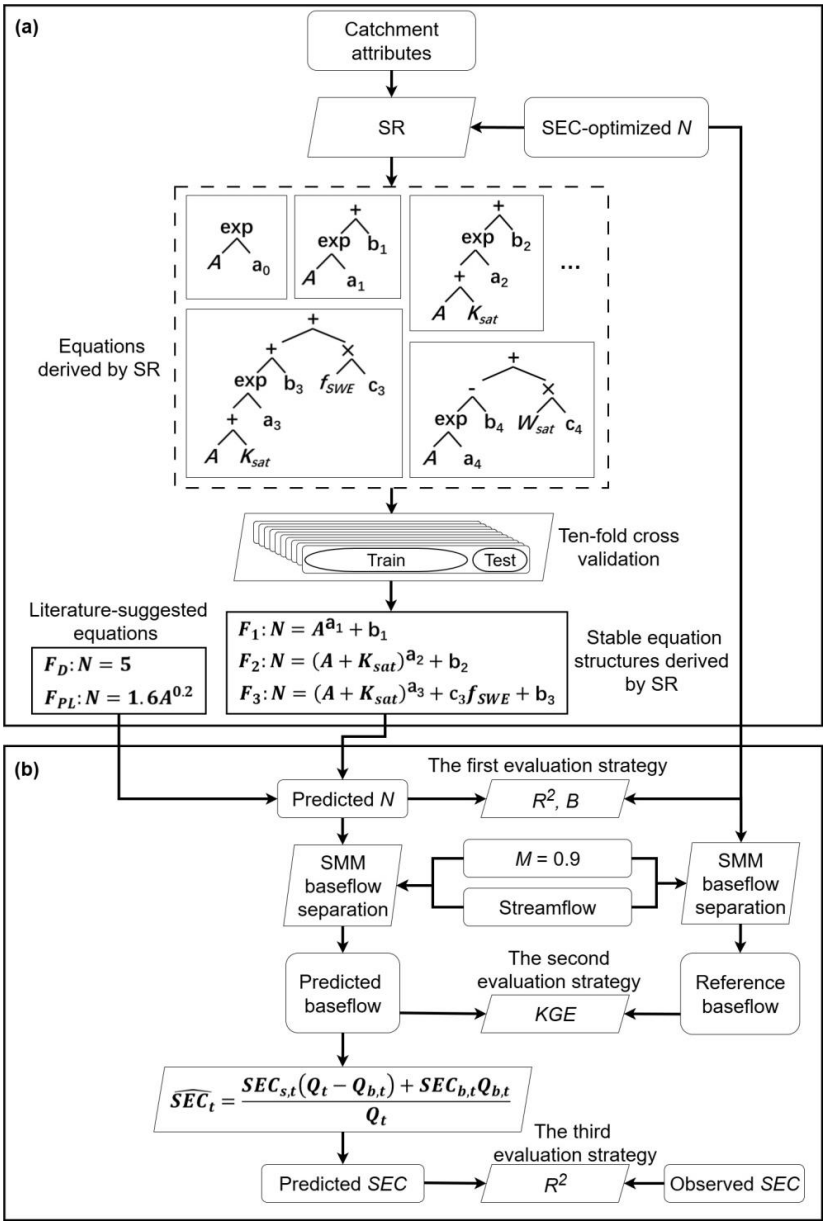


**Figure 2. Flowchart of the SR-based prediction framework for the parameter *N* of SMM (a) and the three performance evaluation strategies (b).**

### 3.3. Evaluation strategies

Three strategies are employed to evaluate the performance of different *N*s calculated by the SR formulas (**Figure 2**b). The first strategy compares the predicted and reference *N*s using the mean bias ($B$) and coefficient of determination ($R^2$):

https://doi.org/10.5194/egusphere-2025-6011
Preprint. Discussion started: 12 December 2025


$$B = \frac{1}{C}\sum_{i=1}^{C}\left(N_i - \hat{N}_i\right) \quad , \qquad (2)$$

$$R^2 = \frac{\sum_{i=1}^{C}(N_i - \bar{N}_r)^2 - \sum_{i=1}^{C}\left(N_i - \hat{N}_i\right)^2}{\sum_{i=1}^{C}(N_i - \bar{N}_r)^2} \quad , \qquad (3)$$

where $\bar{N}_r = \frac{1}{C}\sum_{i=1}^{C} N_i$ is the mean of the reference $N$ over all catchments. Positive (negative) $B$ s indicate overestimation (underestimation), with lower magnitudes suggesting better performance. $R^2$ measures the proportion of variance explained by the prediction; it ranges from 0 to 1, with higher values indicating better agreement.

The second strategy evaluates the SR-derived $N$ values in the context of baseflow separation using the SMM method. Specifically, the SMM baseflow time series are calculated using different $N$ values with the other parameter $M$ fixed at 0.9 to eliminate its influence. Baseflow time series calculated with the reference $N$ for each catchment ($N_i$) is used as the reference. The similarity between the calculated and reference baseflow is assessed using the Kling-Gupta Efficiency (KGE) metric (Gupta et al., 2009):

$$KGE = 1 - \sqrt{(\rho - 1)^2 + \left(\frac{\sigma_p}{\sigma_r} - 1\right)^2 + \left(\frac{\mu_p}{\mu_r} - 1\right)^2} \quad , \qquad (4)$$

where $\rho$ is the correlation coefficient between the predicted and reference baseflow, and $\mu$ and $\sigma$ denote the mean and standard deviation of baseflow. KGE ranges from negative infinity to 1, with higher values indicating better agreement.

The third strategy compares SEC calculated using the SMM baseflow with the observed SEC. Specifically, baseflow time series generated by SMM using $N$s derived by the constant, the power-law, and the three SR formulas are used to estimate SEC based on the chemical and water balance relationship:

$$\widehat{SEC_t} = \frac{SEC_{s,t}(Q_t - B_t) + SEC_{b,t}B_t}{Q_t} \quad , \qquad (5)$$

where $Q_t$ and $B_t$ are the observed streamflow and the predicted baseflow at time $t$, respectively; $SEC_{s,t}$ and $SEC_{b,t}$ are the surface flow and baseflow SEC concentrations, respectively. The values of $SEC_{s,t}$ and $SEC_{b,t}$ are derived using the extreme value interpolation method, which connects the monthly maxima and minima of the observed SEC with spline interpolation to represent the stable variation of SEC in each of the flow components (Mei et al., 2024a). The derivation of Eq. 5 is documented in Appendix A of the Supporting Information. The agreement between observed and predicted streamflow SEC is assessed using the $R^2$ metric (Eq. 1).

## 4. Results

### 4.1. SR expressions for $N$ predictions

Three SR expressions with identical structures and increasing complexity of 5, 7, and 11 occurred consistently across the ten iterations of the cross-validation. They are $N = A^{a_1} + b_1$, $N = (A + K_{sat})^{a_2} + b_2$, and $N = (A + K_{sat})^{a_3} + c_3 \cdot f_{SWE} + b_3$, where $a$, $b$, and $c$ are constants that exhibit minor variation among iterations (see

https://doi.org/10.5194/egusphere-2025-6011
Preprint. Discussion started: 12 December 2025


**Table 2** for details). This consistency suggests that these three forms are robust for the predictions of $N$. Therefore, our analysis focuses on these formulas, which are hereafter referred to as $F_1$, $F_2$, and $F_3$, respectively.

**Table 2. The three stable forms of SR expressions across all ten iterations of the cross-validation. The numbers within the brackets of the first row are the complexity indices of the expressions.**

| Iteration | $F_1$ (5) | $F_2$ (7) | $F_3$ (11) |
|---|---|---|---|
| 1 | $A^{0.23} + 3.77$ | $(A + K_{sat})^{0.24} + 1.66$ | $(A + K_{sat})^{0.24} + 3.05 f_{SWE} + 0.70$ |
| 2 | $A^{0.23} + 3.70$ | $(A + K_{sat})^{0.24} + 1.79$ | $(A + K_{sat})^{0.24} + 3.12 f_{SWE} + 1.22$ |
| 3 | $A^{0.23} + 3.80$ | $(A + K_{sat})^{0.24} + 1.76$ | $(A + K_{sat})^{0.24} + 3.18 f_{SWE} + 0.76$ |
| 4 | $A^{0.23} + 3.67$ | $(A + K_{sat})^{0.24} + 1.95$ | $(A + K_{sat})^{0.24} + 3.18 f_{SWE} + 1.03$ |
| 5 | $A^{0.23} + 3.70$ | $(A + K_{sat})^{0.24} + 1.81$ | $(A + K_{sat})^{0.24} + 3.39 f_{SWE} + 1.01$ |
| 6 | $A^{0.23} + 3.74$ | $(A + K_{sat})^{0.25} + 1.79$ | $(A + K_{sat})^{0.24} + 4.12 f_{SWE} + 0.80$ |
| 7 | $A^{0.23} + 3.65$ | $(A + K_{sat})^{0.24} + 1.90$ | $(A + K_{sat})^{0.24} + 3.20 f_{SWE} + 1.25$ |
| 8 | $A^{0.23} + 3.61$ | $(A + K_{sat})^{0.24} + 1.90$ | $(A + K_{sat})^{0.24} + 3.44 f_{SWE} + 1.17$ |
| 9 | $A^{0.23} + 3.73$ | $(A + K_{sat})^{0.24} + 1.87$ | $(A + K_{sat})^{0.24} + 3.26 f_{SWE} + 1.20$ |
| 10 | $A^{0.23} + 3.75$ | $(A + K_{sat})^{0.24} + 1.84$ | $(A + K_{sat})^{0.24} + 3.23 f_{SWE} + 1.02$ |

Formula $F_1$ predicts $N$ by $A$ with a power-law function with identical exponents (0.23) and nearly identical intercepts (3.61-3.80 days, **Table 2**). These consistent coefficients result in nearly identical relationship across the ten $F_1$s that $N$ increases exponentially with $A$ at a diminishing rate (**Figure 3**a). Formula $F_2$ incorporates both $A$ and $K_{sat}$ in similar power-law functions with nearly identical exponents (0.24-0.25) and intercepts (1.66-1.95 days, **Table 2**). Increases in either variable contribute to higher values of $N$ (**Figure 3**b and c). However, the relative importance of these predictors is modulated by their interaction: when $A$ is large, the influence of $K_{sat}$ becomes minimal; conversely, when $A$ is small, the contribution of $K_{sat}$ is more pronounced. This interaction also explains the observed patterns in **Figure 3**a and b, where $F_1$ and $F_2$ show clear dependence on catchment area when $A < 1000$ km$^2$. Formula $F_3$ extends $F_2$ by adding $f_{SWE}$ as a linear term. The 10 replicated formulas still reveal nearly identical exponents (0.24), slopes (3.05-4.12 days, **Table 2**), and intercepts (0.70-1.25 days). The marginal relationships of $N$ with $A$ and $K_{sat}$ mirror those of $F_2$ (**Figure 3**d and e). As for $f_{SWE}$, larger values lead to higher prediction with a constant rate of 0.3-0.4 days per 0.1 fraction increases as indicated by the linear relationship (**Figure 3**f). Overall, SR identifies $A$ as the most influential factor in predicting $N$, as evidenced by its presence in all SR-derived formulas. The narrower ranges of predicted $N$s in **Figure 3**b and d also suggest that $A$ exerts greater influence than $K_{sat}$ and $f_{SWE}$.

https://doi.org/10.5194/egusphere-2025-6011
Preprint. Discussion started: 12 December 2025


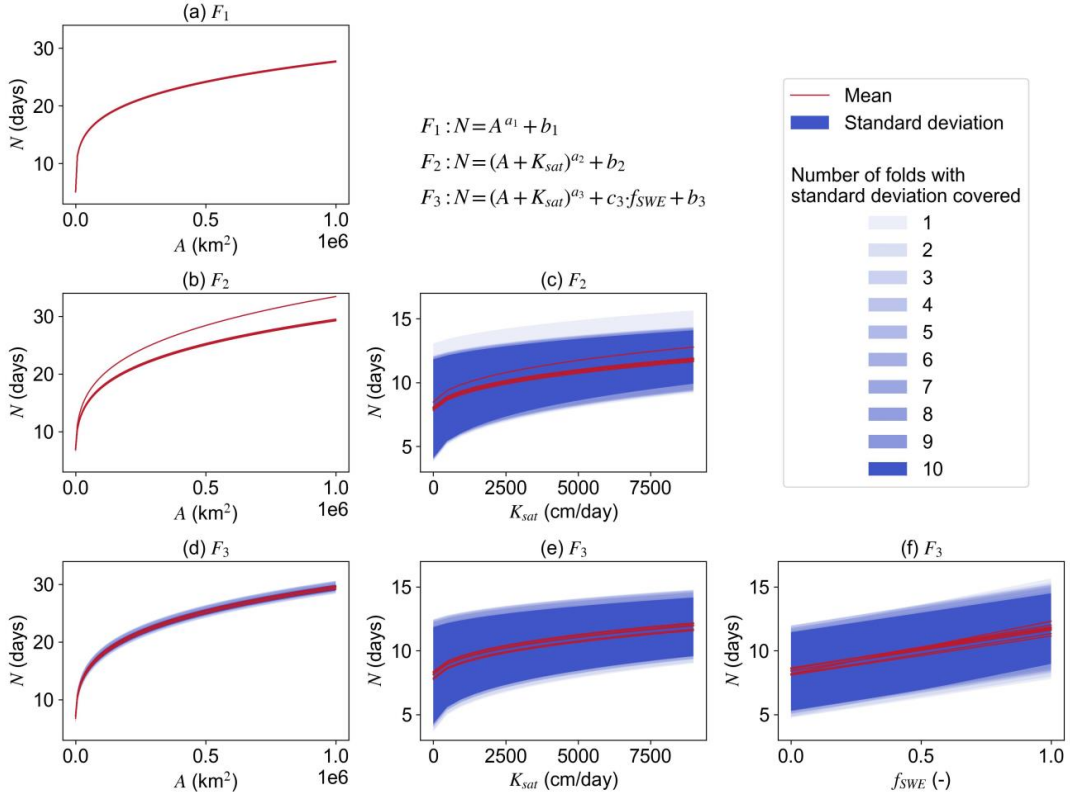


**Figure 3. Marginal relationship of $N$ on different predictors ($A$, $K_{sat}$, and $f_{SWE}$) that consist of the SR expressions ($F_1$, $F_2$, and $F_3$). Each line represents one of the ten instances of $F_1$, $F_2$, and $F_3$. Panels a, b, and d are for $A$; panels c and e are for $K_{sat}$; panel f is for $f_{SWE}$.**

### 4.2. Evaluation of $N$ predictions

**Figure 4** presents the performance of $N$ predicted using the two literature-suggested formulas ($F_D$ and $F_{PL}$) and the three SR formulas ($F_1$, $F_2$, and $F_3$) for the ten training and testing sets. It should be noted that the literature-suggested formulas do not require training; instead, they are directly applied to the training and testing sets separately. Overall, the performance of formula $F_D$ is poor, with negative $R^2$ values less than -0.6. $F_{PL}$ shows improved performance but still yields modest $R^2$ medians of 0.23 and 0.22 for the training and testing sets, respectively. The predictions of $N$ based on the three SR-derived formulas significantly outperform those based on the two literature-suggested formulas. The $R^2$ medians for $F_1$, $F_2$, and $F_3$ are 0.49, 0.52, and 0.55 for the training sets, and 0.46, 0.49, and 0.54 for the testing sets, respectively. The overall $R^2$ values for the ten testing sets together for $F_1$, $F_2$, and $F_3$ are 0.49, 0.50, and 0.54, respectively. In terms of the bias, the SR-derived formulas significantly reduce the underestimation of $N$ by the literature-suggested formulas (**Figure 4**b). The medians $B$ for $F_1$, $F_2$, and $F_3$ are –0.05/0.01 days, –0.18/–0.13 days, and 0.00/0.01 days for the training/testing sets, respectively, comparing to $F_D$ and $F_{PL}$ at -4.44/-4.38 days and -2.34/-2.28 days. These values for the combined testing set are -4.44, -2.33, -0.05, -0.14 and -0.06 days for $F_D$, $F_{PL}$, $F_1$, $F_2$, and $F_3$, respectively. It is noteworthy that the testing sets exhibit wider ranges of

https://doi.org/10.5194/egusphere-2025-6011
Preprint. Discussion started: 12 December 2025


$R^2$ and $B$ values compared to the training sets. This variability is primarily attributed to the differences in catchment attributes of the testing samples rather than the discrepancies among the 10 replicated formulas. This is supported by the nearly identical coefficients (i.e., $a$, $b$, and $c$) in the SR formulas (**Table 2**).

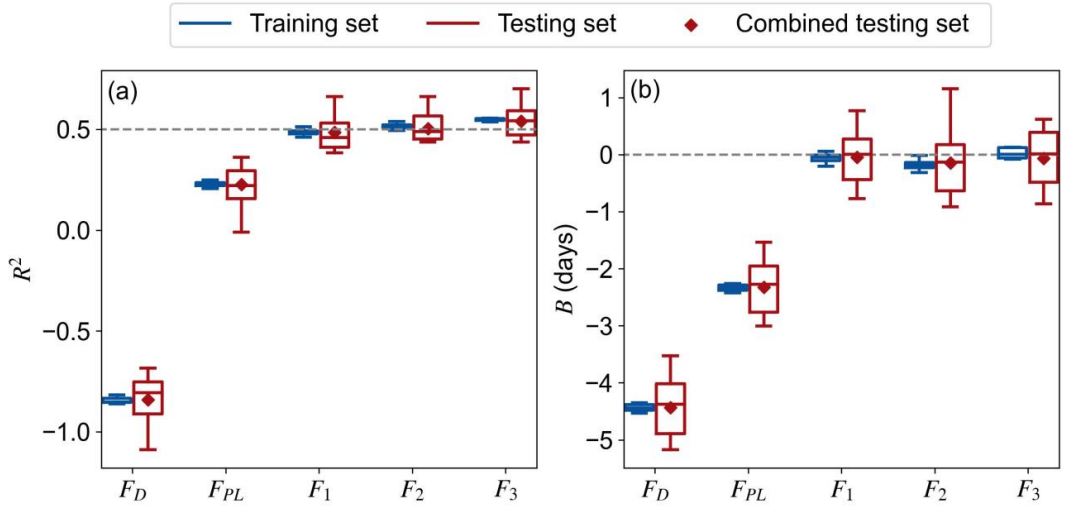


**Figure 4. Performance of $N$ predictions using the constant ($F_D$), power-law ($F_{PL}$), and the three SR formulas ($F_1$, $F_2$, and $F_3$) for the ten training and testing sets of the 10-fold cross-validation: coefficient of determination $R^2$ (a) and mean bias $B$ (b).**

### 4.3. Application of $N$ predictions in baseflow separation

**Figure 5**a reveals the baseflow separation performance of different $N$ predictions measured by KGE for the testing sets. The baseflow separation performance roughly follows the ranking of $F_D < F_{PL} < F_1 < F_2 < F_3$, in line with the $N$ predictions (**Figure 4**). The median KGEs for $F_D$, $F_{PL}$, $F_1$, $F_2$, and $F_3$ are 0.63, 0.73, 0.84, 0.84, and 0.85, respectively. For $F_D$ and $F_{PL}$, 12% and 5% of catchments exhibit KGE < 0, while 64% and 78% report KGE > 0.5, respectively. In contrast, the percentage of catchments with KGE < 0 drops to 1% for $F_1$, $F_2$, and $F_3$, and those with KGE > 0.5 rise to more than 87%. **Figure 5**b shows the performance of the three SR formulas across the 18 HUC2 regions. Overall, all formulas perform well for the HUC2 regions, with median KGEs ranging from 0.61 to 0.93. The best performing regions for $F_1$, $F_2$, and $F_3$ are HUC 02, 01, and 07, respectively, exhibiting median KGE values above 0.89 and over 95% of catchments achieving KGE values greater than 0.5. In contrast, the lowest performance for all three formulas occurs in HUC 12, where median KGE values fall below 0.65 and more than 25% of catchments show KGE values below 0.5. All three formulas exhibit larger performance variability in HUC 10-12 and 14 compared to other regions. This can be attributed to the fact that these regions are mountainous and plain areas, characterized by relatively high heterogeneity in catchment characteristics. **Figure 5**c compares the relative performance of $F_1$, $F_2$, and $F_3$ across regions. $F_2$ outperforms $F_1$ for HUC 04-09 located in the northern and northeastern CONUS, while it performs worse than $F_1$ in HUC 12-15 on the south. $F_3$ generally outperforms $F_2$ in the mountainous region spanning HUC 10-11 and 13-18, and shows comparable performance to $F_2$ in HUC 01, 02, 04, 05, and 07 with mild topography.

https://doi.org/10.5194/egusphere-2025-6011
Preprint. Discussion started: 12 December 2025


In HUC 02, 04, 07, 10, 11, 13, 14, 16, and 18, the most complex $F_3$ outperforms the other SR formulas. However, $F_3$ performs worse than $F_1$ and $F_2$ in HUC 06 and 12. This is because these SR formulas were fitted using data from all catchments, aiming to achieve optimal performance at a global scale. As a result, it may involve trade-offs that reduce its effectiveness in specific catchments.

https://doi.org/10.5194/egusphere-2025-6011
Preprint. Discussion started: 12 December 2025


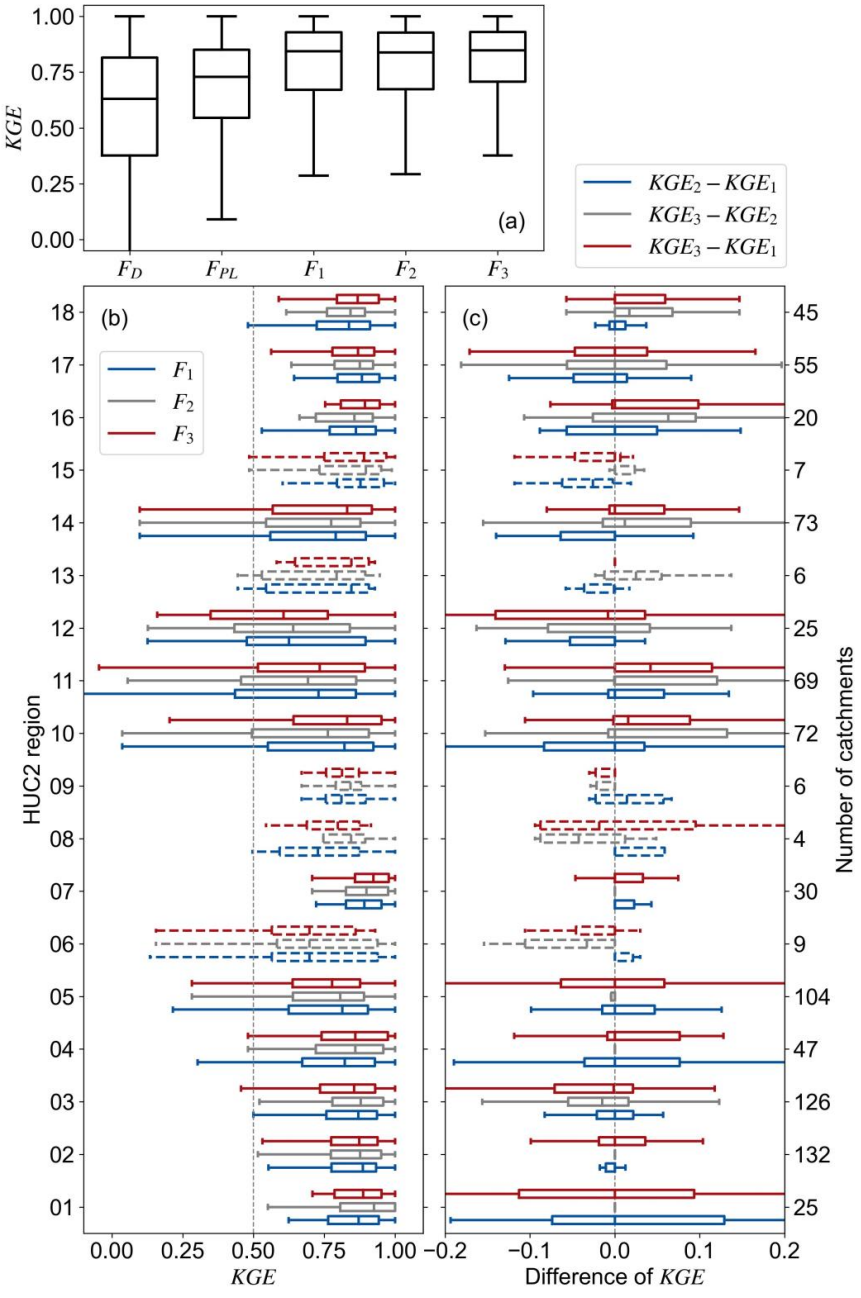


**Figure 5. Baseflow separation performance based on different *N* predictions for all catchments (a) and for the 18 HUC2 regions (b), and relative performance between each pair of the three SR cases for the HUC2 regions (c). Regions with fewer than 10 catchments are indicated by dashed lines in panels b and c.**

https://doi.org/10.5194/egusphere-2025-6011
Preprint. Discussion started: 12 December 2025


**Figure 6** presents the average KGE of baseflow separation as functions of the three influential catchment attributes. Overall, the SR formulas consistently outperform the literature-suggested formulas for most of the predictor value ranges, with relatively minor performance differences among $F_1$, $F_2$, and $F_3$, highlighting their robustness across diverse catchment conditions. According to **Figure 6**a, when $A$ exceeds 300 km$^2$, corresponding to $N = 5$ days by $F_{PL}$, the performance of $F_D$ deteriorates markedly. This suggests that using $N = 5$ days cannot adequately represent its variation for larger $A$s. Conversely, for $A < 300$ km$^2$, the performance of $F_{PL}$ declines, indicating that the power function coefficients are not suitable for smaller catchments over CONUS. Across the full range of $A$, the SR formulas consistently achieve higher KGE values, emphasizing the benefits of regional calibration. For small catchment ($A <$ 100 km$^2$), accounting for $f_{SWE}$ and $K_{sat}$ leads to performance gains. In contrast, for larger basins ($A > 100$ km$^2$), the additional contribution of these factors becomes negligible. **Figure 6**b examines the influence of $K_{sat}$. When $K_{sat} <$ 5 mm/hour, all predictions show similar level of baseflow prediction performance, suggesting that $K_{sat}$ is not a major factor in these regions. However, when $K_{sat} > 25$ mm/hour, incorporating $K_{sat}$ substantially improves the predictions, highlighting its influence for catchments with high averaged-permeability. In the intermediate ranges (5–25 mm/hour), the regionally fitted power-law formula ($F_1$) outperforms the literature-suggested power-law formula ($F_{PL}$). Although $F_1$ does not explicitly include $K_{sat}$, its performance remains comparable to $F_2$ and $F_3$, which incorporate $K_{sat}$. This indicates that regional fitting may compensate the effects of $K_{sat}$. **Figure 6**c reveals the influence of $f_{SWE}$. $F_3$ outperforms $F_1$ and $F_2$ when $f_{SWE} > 0.4$, indicating that catchments strongly influenced by snow exhibit lower performance if $f_{SWE}$ is not accounted for, thereby underscoring its substantial effect on $N$. In contrast, for $f_{SWE} < 0.4$, $F_1$ and $F_2$ perform similarly to $F_3$, demonstrating that regionally calibrated coefficients can partially offset the lack of explicit consideration of snow-related variables.

https://doi.org/10.5194/egusphere-2025-6011
Preprint. Discussion started: 12 December 2025


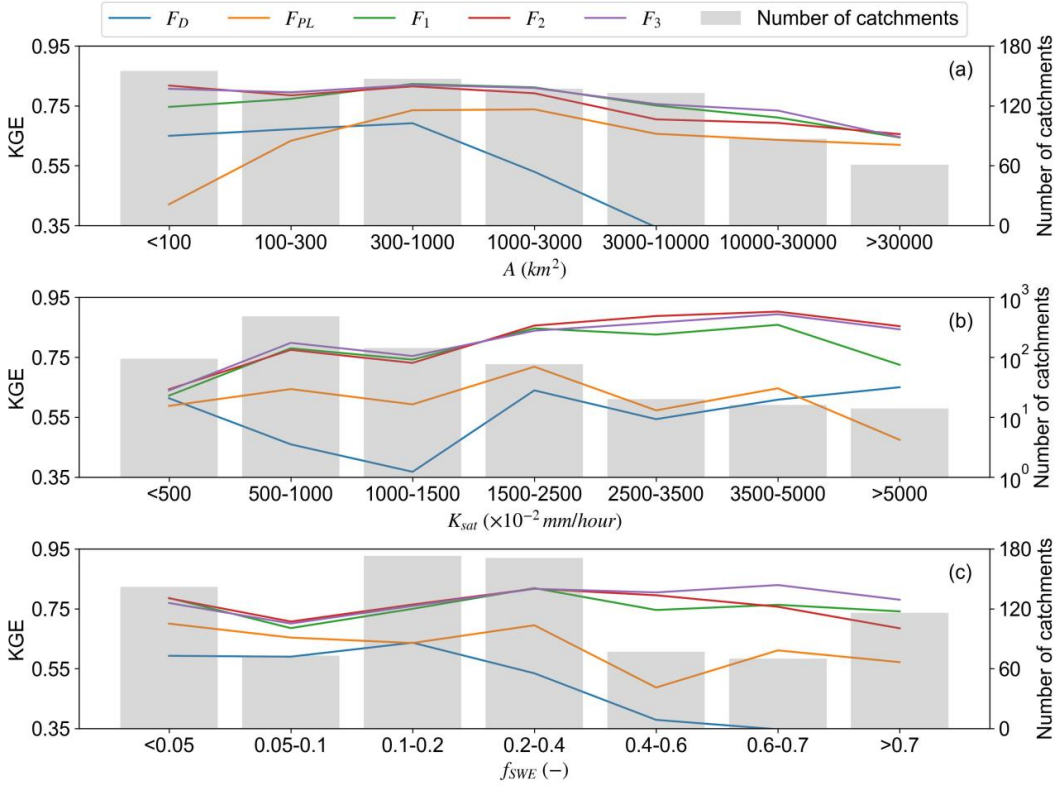


**Figure 6. Performance of baseflow separation for different ranges of catchment area (a), catchment-averaged saturated hydraulic conductivity (b), and snow day fraction (c). The right y-axis for panel b is in logarithmic scale.**

### 4.4. Estimation of SEC variation based on predicted *N*ss

**Figure 7** reveals the performance of SEC estimations by different $N$ predictions for the testing sets. The overall distribution (**Figure 7**a) reveals that the ranking of performance follows the order $F_D < F_{PL} < F_1 < F_2 < F_3$, consistent with the $N$ predictions (**Figure 4**) and baseflow separation results (**Figure 5**). The medians of $R^2$ stay closed from 0.70 to 0.74, with similar interquartile ranges from 0.29 to 0.33. **Figure 7**b illustrates the spatial distribution of the best-performing formulas across the HUC4 regions. $F_3$ demonstrates superior performance across most of the mountainous regions, including the Rocky Mountain foothills, Cascade Range, Sierra Nevada, and some regions within the Great Plains. The improvement for the mountainous regions is likely due to the explicit incorporation of $f_{SWE}$ in the SR formula, capturing the influence of snow processes; for the relatively flat Great Plains regions, the improvement is primarily driven by the consideration of $K_{sat}$, which better represents subsurface processes such as infiltration capacity, percolation, and lateral subsurface flow that regulate groundwater recharge and baseflow contributions. In contrast, $F_1$ performs best in the eastern and southeastern CONUS, including the Appalachian Mountains, coastal plain, and Florida peninsular, where the effects of $K_{sat}$ and $f_{SWE}$ are minimal. These regions are generally characterized by low BFI values (**Figure 1**c), indicating surface runoff-dominated streamflow with limited relevance of delayed-flow processes (McMillan, 2020; Wu et al., 2021).

https://doi.org/10.5194/egusphere-2025-6011
Preprint. Discussion started: 12 December 2025


$F_2$ achieves the highest performance in fewer HUC4 regions, indicating that the effects of $K_{sat}$ may be compensated by the regional calibration of $F_1$. Interestingly, several regions located in the Great Plains exhibit mixed optimal performance for multiple formulas, most frequently $F_2$ and $F_3$, suggesting a more complex interplay of hydrological drivers in these areas.

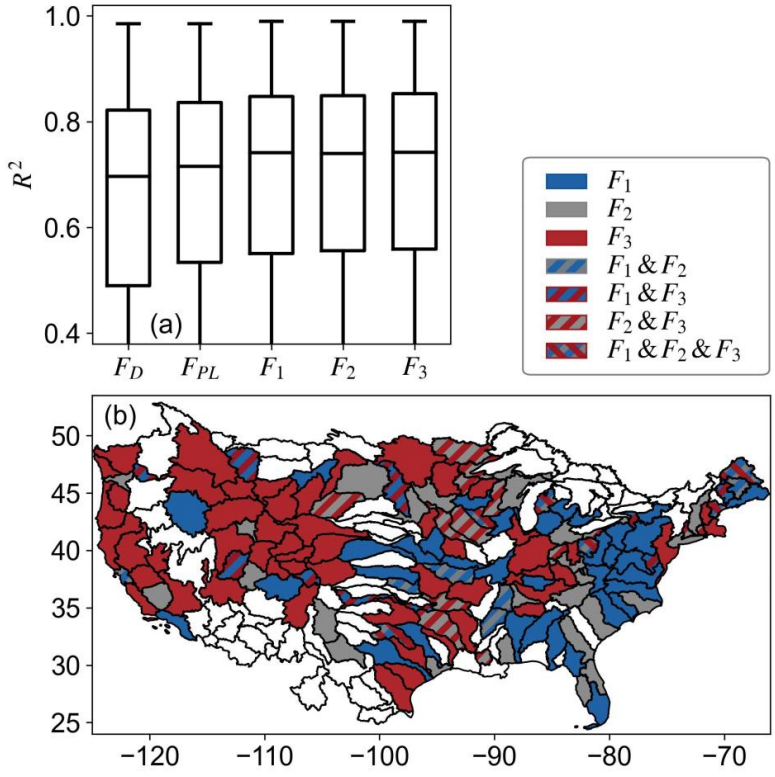


**Figure 7. Performance of SEC estimations by different *N* predictions for all catchments (a) and the spatial distribution of the best-performing formulas across different HUC4 regions (b). The best-performing formula for a HUC4 region is determined based on the average $R^2$ of all sites within the region.**

## 5. Discussions

### 5.1. Regionalization of baseflow separation parameter by SR

In this study, we identify three mathematical expressions for the predictions of *N* with identical structures and predictors and almost identical regression coefficients using SR. Compared to the RF-based prediction of *N* (Lin et al., 2025b), the SR-based approach provides lower predictive skill ($R^2$ = 0.54 vs. 0.80), but allows us to quantify how catchment attributes (i.e., catchment area, saturated hydraulic conductivity, and snow day fraction) influence baseflow separation (Häfner et al., 2023; Karpatne et al., 2024). For instance, by differentiating $F_3$, we obtain the marginal effects of each attribute on $N$: $\frac{\partial N}{\partial A} = a_3\ (A + K_{\text{sat}})^{\,a_3-1}$, $\frac{\partial N}{\partial K_{\text{sat}}} = a_3\ (A + K_{\text{sat}})^{\,a_3-1}$, and $\frac{\partial N}{\partial f_{\text{SWE}}} = c_3$. These

https://doi.org/10.5194/egusphere-2025-6011
Preprint. Discussion started: 12 December 2025


derivatives quantify the sensitivity of $N$ to individual catchment attributes and facilitate a clearer interpretation of the underlying functional relationships.

One important aspect to consider when training SR models is the diversity of mathematical operators. A wide variety of operators for model training enables the discovery of complex relationships among variables, but it also enlarges the search space, increasing training time and risk of overfitting (Elsken et al., 2019; Li et al., 2025). To address these challenges, we adopted two strategies. First, we incorporated domain knowledge to guide the choice of operators. Specifically, the well-established power-law relationship between streamflow response time and catchment area motivated the inclusion of the exponential operator in the SR operator set. The fact that all SR-derived formulas captured this power-law relationship indicates that the use of domain knowledge was effective. Second, cross-validation was applied to assess model generalizability and reduce overfitting, ensuring representativeness of the SR expressions across the diverse catchments. Although SR can generate more complex formulas than $F_3$ with better training fit, these structures are inconsistent across folds. This suggests that they may overfit specific subsets of the data and lack generalizability, and are therefore excluded from our analysis.

### 5.2. Influential catchment attributes for $N$ predictions

The segment length parameter $N$ is a proxy of the average duration of surface flow, and larger values indicate surface flow of event sustain for longer time on average (Stoelzle et al., 2020). Our findings indicate that $N$ is a power function of catchment area with exponent of 0.23-0.25 (**Table 2**), indicating that larger catchments are characterized by longer average surface flow duration (Garzon et al., 2023; Mei and Anagnostou, 2015), and the increasing rate in duration slows down for larger $A$s. This could be attributed to the longer averaged water paths for larger catchments (i.e., the Hack's Law), increasing the average traveling time for surface flow of event (Tarasova et al., 2024). Saturated hydraulic conductivity is another key factor in the predictions of $N$: $N$ increases according to the power-law functions with exponents of 0.24-0.25 with respect to the sum of $K_{sat}$ and $A$ ($F_2$ and $F_3$ in **Table 2**). This indicates that higher $K_{sat}$values tend to increase the average duration of surface flow with decreasing rate. A possible explanation is that catchments with higher $K_{sat}$ tend to promote infiltration, making more rainfall excess to rout through the slow subsurface flow paths than the rapid overland ones (Nagy et al., 2024). $F_3$ reveals that prolonged snow cover (higher fraction of days covered by snow) is linearly associated with longer surface flow duration. This is due to the snowpack acting as a seasonal storage that modulates streamflow timing (Stoelzle et al., 2020). The gradual melting of snowpack slowly released meltwater to the stream networks, increasing the time needed to leave the catchment (Barnhart et al., 2016; Godsey et al., 2014; Noor et al., 2023).

### 5.3. Trade-off between formula complexity and prediction accuracy

Our experiments reveal that formulas for baseflow separation with higher complexity tend to achieve better predictive performance. This is because more complex formulas can incorporate additional predictors for more detailed descriptions of the underlying hydrological processes. However, in some cases, simpler formulas yield comparable performance to more complex formulas. For example, when $K_{sat}$ and $f_{SWE}$ take relatively small values ($K_{sat} < 25$ mm/hour and $f_{SWE} < 0.4$), the performance differences among $F_1$, $F_2$, and $F_3$ are minimal (**Figure 6**).

https://doi.org/10.5194/egusphere-2025-6011
Preprint. Discussion started: 12 December 2025


This is likely because small variations in $K_{sat}$ and $f_{SWE}$ have limited impact to the prediction, allowing the regional calibration to partially compensate for the absence of these variables in the formulas. However, such compensation is limited for large $K_{sat}$ and $f_{SWE}$ ($K_{sat} > 25$ mm/hour and $f_{SWE} > 0.4$), where their influence becomes more pronounced. Moreover, the effects of $K_{sat}$ and $f_{SWE}$ are more evident when catchment area is small ($A < 100$ km$^2$). As catchment area increases ($A > 100$ km$^2$), their influence is outweighed by $A$, highlighting the dominant role of drainage area in shaping the streamflow response time (**Figure 6a**).

## 6. Conclusions and future work

In this study, we applied symbolic regression to derive formulas for the prediction of segment length parameter $N$ (a proxy of the average duration of surface flow) of the smooth minima baseflow separation method across 855 CONUS catchments. Three stable formulas with increasing complexity were identified: $N = A^{a_1} + b_1$, $N = (A + K_{sat})^{a_2} + b_2$, and $N = (A + K_{sat})^{a_3} + c_3 \cdot f_{SWE} + b_3$, where catchment area ($A$), saturated hydraulic conductivity ($K_{sat}$), and snow day fraction ($f_{SWE}$) are identified as important predictors. These SR formulas showed substantial improvements in predictive accuracy of $N$ comparing to the constant ($N = 5$) and power-law formula ($N = 1.6A^{0.2}$). The SR-derived $N$s also reveal better performance in baseflow separation and in estimation of electrical conductance dynamics. Among the three SR formulas, $F_3$ performs better in regions influenced by snow, such as the mountainous mid-west and the northern CONUS; $F_1$ shows better performance in the eastern and southeastern CONUS, where both the climate and terrain are mild and infiltration rate is low. Overall, formulas that consider $K_{sat}$ and $f_{SWE}$ tend to yield higher predictive accuracy, but simpler formulas without $K_{sat}$ or $f_{SWE}$ can still achieve comparable performance when the values of these key predictors are relatively small. This study presents a new paradigm for regionalization of optimal baseflow parameters using symbolic regression and demonstrates its potential to improve model interpretability and transferability across diverse catchments.

This study used all gages across CONUS to train SR. However, the influence of catchment attributes on $N$ varies across regions (**Figure 7**). Future work could explore the benefits of developing region-specific SR formulas for different catchment clusters to improve the prediction performance. Furthermore, this study investigated SR-based modeling of only one parameter of a baseflow separation method. Future research could explore applying SR to other baseflow separation methods to identify the governing equations relating catchment attributes to the parameters of these methods. This may help to understand how catchment attributes influence the partitioning of streamflow.

## Appendix A: Calculate SEC based on chemical and water balance relationship

For a two-component streamflow composition scenario, in which total streamflow is composed of a rapid surface/shallow subsurface flow component and a slower baseflow component, the mass balance relationships can be expressed as:

$$SEC_t Q_t = SEC_{s,t} S_t + SEC_{b,t} B_t \quad , \qquad (A1)$$

$$Q_t = S_t + B_t \quad , \qquad (A2)$$

https://doi.org/10.5194/egusphere-2025-6011
Preprint. Discussion started: 12 December 2025


where $Q_t$ and $SEC_t$ denote the total streamflow and the corresponding environmental tracer concentration at time step $t$, respectively. $S_t$ and $B_t$ are the surface flow and baseflow contributions at time step $t$. $SEC_{s,t}$ and $SEC_{b,t}$ are the tracer concentration of surface flow and baseflow.

Combining equations (A1) and (A2), we obtain:

$$SEC_t Q_t = SEC_{s,t}(Q_t - B_t) + SEC_{b,t}B_t \quad (A3)$$

Dividing both sides by $Q_t$ yields:

$$SEC_t = \frac{SEC_{s,t}(Q_t - B_t) + SEC_{b,t}B_t}{Q_t}, \quad (A4)$$

**Appendix B:**

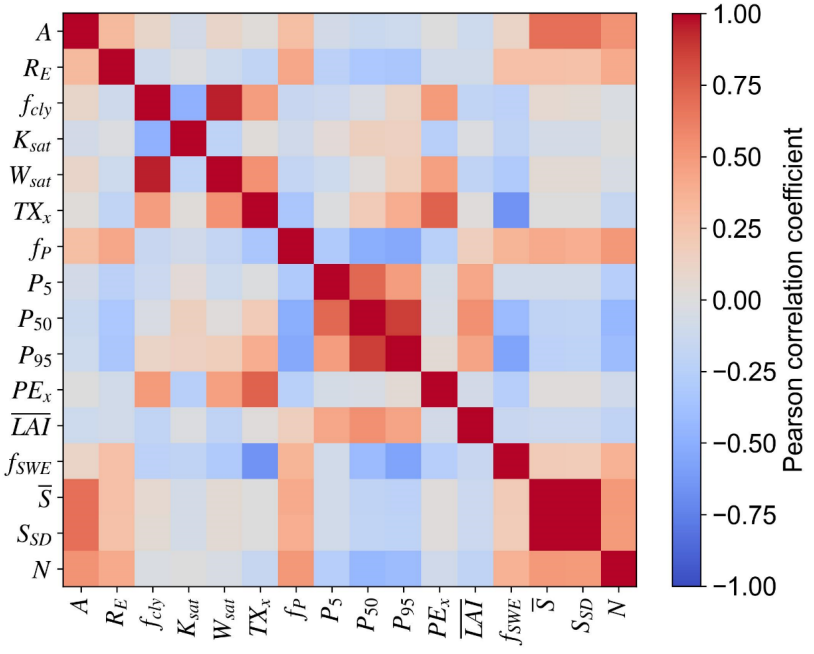


**Figure B1. Pearson correlation coefficients between 15 catchment characteristics and the segment length parameter *N* of SMM.**

https://doi.org/10.5194/egusphere-2025-6011
Preprint. Discussion started: 12 December 2025


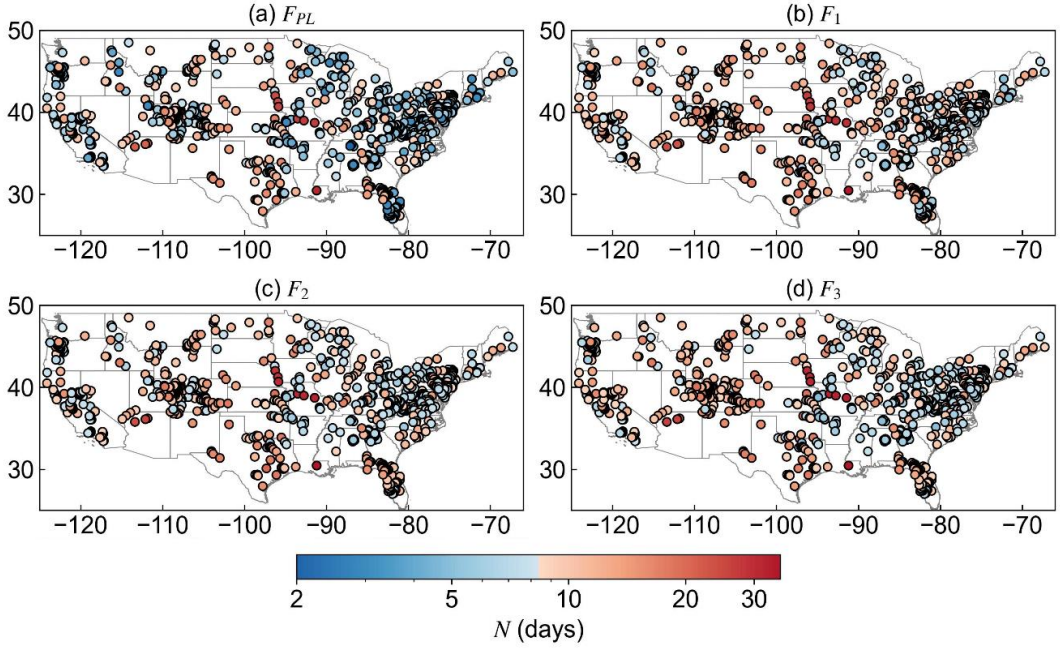


**Figure B2. Spatial distributions of the *N* parameter predicted by the power-law function relationship with drainage area (a) and three SR-derived formulas (b-d).**

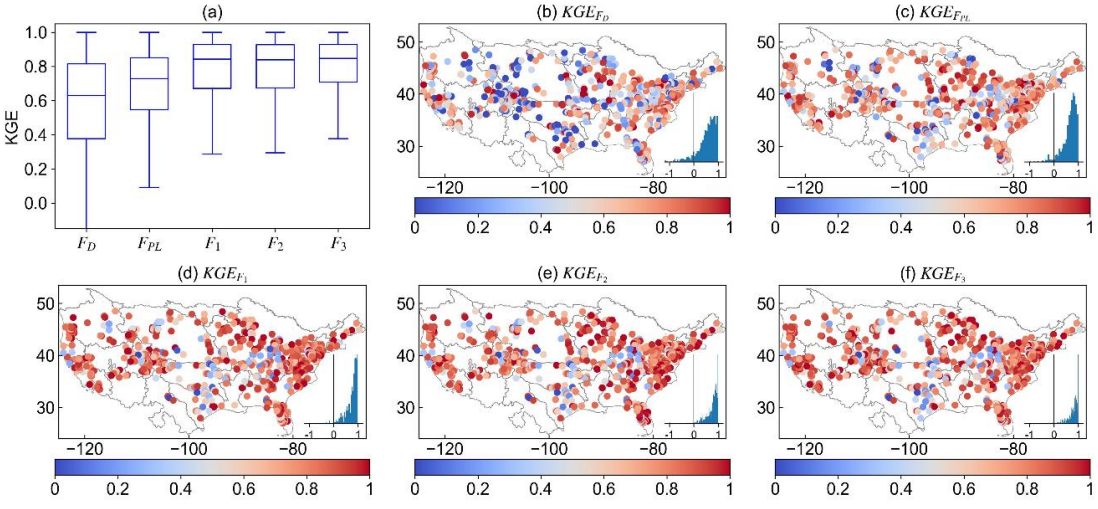


**Figure B3. Spatial distributions of baseflow separation performance measured by KGE for SMM with different parameterizations of *N*.**

**Financial support.** This work is supported by the National Natural Science Foundation of China (52579030) and the Guangdong Natural Science Foundation (2025A1515011666 and 2025A1515012264).

https://doi.org/10.5194/egusphere-2025-6011
Preprint. Discussion started: 12 December 2025


**Competing interests.** The authors declare that they have no conflict of interest.

**Code and data availability.** The streamflow and baseflow time series and optimal baseflow filters parameters are available on Mei et al. (2024b). The HUC region maps are downloaded from Climate Mapping for Resilience & Adaptation (CMRA). The catchment attributes of the 855 catchments are available on Lin et al. (2025a).

**Author contributions.** Yongen Lin: Conceptuation, Methodology, Data curation, Formal analysis, Visualization, investigation, validation, writing–original draft; Dagang Wang: Conceptuation, Methodology, Writing–review & editing, supervision, Resources, funding acquisition, project administration; Yiwen Mei: Conceptuation, Methodology, Writing–review & editing, supervision, Resources, funding acquisition; Jinxin Zhu: Methodology, Writing–review & editing; Huan Wu: Funding acquisition, Writing–review & editing; Shuo Wang: Writing–review & editing; Zhonghou Xu: Resources, Writing–review & editing; Asaad Y. Shamseldin: Resources, Writing–review & editing; Emmanouil N. Anagnostou: Writing–review & editing.

## References

Aksoy, H., Unal, N.E., Pektas, A.O., 2008. Smoothed minima baseflow separation tool for perennial and intermittent streams. Hydrological Processes, 22(22): 4467-4476. DOI:https://doi.org/10.1002/hyp.7077

Barnhart, T.B. et al., 2016. Snowmelt rate dictates streamflow. Geophysical Research Letters, 43(15): 8006-8016. DOI:https://doi.org/10.1002/2016GL069690

Cartwright, I., 2022. Implications of variations in stream specific conductivity for estimating baseflow using chemical mass balance and calibrated hydrograph techniques. Hydrology and Earth System Sciences, 26(1): 183-195. DOI:10.5194/hess-26-183-2022

Cranmer, M., 2023. Interpretable machine learning for science with PySR and SymbolicRegression. jl. arXiv preprint arXiv:2305.01582.

Elsken, T., Metzen, J.H., Hutter, F., 2019. Neural architecture search: a survey. J. Mach. Learn. Res., 20(1): 1997–2017.

Feigl, M., Herrnegger, M., Klotz, D., Schulz, K., 2020. Function Space Optimization: A Symbolic Regression Method for Estimating Parameter Transfer Functions for Hydrological Models. Water Resour Res, 56(10): e2020WR027385. DOI:10.1029/2020WR027385

Garzon, L.F.L., Johnson, M.F., Mount, N., Gomez, H., 2023. Exploring the effects of catchment morphometry on overland flow response to extreme rainfall using a 2D hydraulic-hydrological model (IBER). Journal of Hydrology, 627: 130405. DOI:https://doi.org/10.1016/j.jhydrol.2023.130405

Gnann, S.J., McMillan, H.K., Woods, R.A., Howden, N.J.K., 2021. Including Regional Knowledge Improves Baseflow Signature Predictions in Large Sample Hydrology. Water Resources Research, 57(2): e2020WR028354. DOI:https://doi.org/10.1029/2020WR028354

Godsey, S.E., Kirchner, J.W., Tague, C.L., 2014. Effects of changes in winter snowpacks on summer low flows: case studies in the Sierra Nevada, California, USA. Hydrological Processes, 28(19): 5048-5064. DOI:https://doi.org/10.1002/hyp.9943

Gupta, H.V., Kling, H., Yilmaz, K.K., Martinez, G.F., 2009. Decomposition of the mean squared error and NSE performance criteria: Implications for improving hydrological modelling. Journal of Hydrology, 377(1-2): 80-91. DOI:10.1016/j.jhydrol.2009.08.003

Gustard, A., Bullock, A.D., Dixon, J.M., 1992. Low Flow Estimation in the United Kingdom.

Häfner, D., Gemmrich, J., Jochum, M., 2023. Machine-guided discovery of a real-world rogue wave model. Proceedings of the National Academy of Sciences, 120(48): e2306275120. DOI:doi:10.1073/pnas.2306275120

Hagedorn, B., 2020. Hydrograph separation through multi objective optimization: Revealing the importance of a temporally and spatially constrained baseflow solute source. Journal of Hydrology, 590: 125349. DOI:https://doi.org/10.1016/j.jhydrol.2020.125349

https://doi.org/10.5194/egusphere-2025-6011
Preprint. Discussion started: 12 December 2025


Hou, X., Xie, D., Feng, L., Shen, F., Nienhuis, J.H., 2024. Sustained increase in suspended sediments near global river deltas over the past two decades. Nature Communications, 15(1): 3319. DOI:10.1038/s41467-024-47598-6

Humphrey, C.E. et al., 2022. Using Automated Seepage Meters to Quantify the Spatial Variability and Net Flux of Groundwater to a Stream. Water Resources Research, 58(6): e2021WR030711. DOI:https://doi.org/10.1029/2021WR030711

Karpatne, A., Jia, X., Kumar, V., 2024. Knowledge-guided machine learning: Current trends and future prospects. arXiv preprint arXiv:2403.15989.

Klotz, D., Herrnegger, M., Schulz, K., 2017. Symbolic Regression for the Estimation of Transfer Functions of Hydrological Models. Water Resources Research, 53(11): 9402-9423. DOI:10.1002/2017wr021253

Koza, J.R., 1994. Genetic programming as a means for programming computers by natural selection. Statistics and Computing, 4(2): 87-112. DOI:10.1007/BF00175355

Kronberger, G., de Franca, F.O., Burlacu, B., Haider, C., Kommenda, M., 2022. Shape-Constrained Symbolic Regression—Improving Extrapolation with Prior Knowledge. Evolutionary Computation, 30(1): 75-98. DOI:10.1162/evco_a_00294

Li, X. et al., 2025. UniSymNet: A Unified Symbolic Network Guided by Transformer. arXiv preprint arXiv:2505.06091.

Lin, Y., Mei, Y., Wang, D., 2025a. Data and code archive for "Regionalization of Optimal Baseflow Separation using Catchment-scale Characteristics", [Dataset]. Zenodo. DOI:https://doi.org/10.5281/zenodo.16924118

Lin, Y. et al., 2025b. Regionalization of Optimal Baseflow Separation using Catchment-scale Characteristics. Water Resources Research, under review.

Liu, Y., Liu, R., Chen, J.M., 2012. Retrospective retrieval of long-term consistent global leaf area index (1981–2011) from combined AVHRR and MODIS data. Journal of Geophysical Research: Biogeosciences, 117(G4). DOI:https://doi.org/10.1029/2012JG002084

Makke, N., Chawla, S., 2024. Interpretable scientific discovery with symbolic regression: a review. Artificial Intelligence Review, 57(1). DOI:10.1007/s10462-023-10622-0

McMahon, T.A., Nathan, R.J., 2021. Baseflow and transmission loss: A review. WIREs Water, 8(4): e1527. DOI:https://doi.org/10.1002/wat2.1527

McMillan, H., 2020. Linking hydrologic signatures to hydrologic processes: A review. Hydrological Processes, 34(6): 1393-1409. DOI:https://doi.org/10.1002/hyp.13632

McMillan, H.K., Gnann, S.J., Araki, R., 2022. Large Scale Evaluation of Relationships Between Hydrologic Signatures and Processes. Water Resources Research, 58(6): e2021WR031751. DOI:https://doi.org/10.1029/2021WR031751

Mei, Y., Anagnostou, E.N., 2015. A hydrograph separation method based on information from rainfall and runoff records. Journal of Hydrology, 523: 636-649. DOI:https://doi.org/10.1016/j.jhydrol.2015.01.083

Mei, Y. et al., 2024a. Optimal Baseflow Separation Through Chemical Mass Balance: Comparing the Usages of Two Tracers, Two Concentration Estimation Methods, and Four Baseflow Filters. Water Resources Research, 60(7). DOI:10.1029/2023wr036386

Mei, Y., Zhu, J., Wang, D., 2024b. Data and Code Archive for "Optimal Baseflow Separation through Chemical Mass Balance: Comparing the Usages of Two Tracers, Two Concentration Estimation Methods, and Four Baseflow Filters", [Dataset]. Zenodo. DOI:https://doi.org/10.5281/zenodo.8388365

Nagy, E.D., Szilagyi, J., Torma, P., 2024. Calibrating the lyne-hollick filter for baseflow separation based on catchment response time. Journal of Hydrology, 638. DOI:10.1016/j.jhydrol.2024.131483

NOHRSC, 2004. Snow Data Assimilation System (SNODAS) Data Products at NSIDC, Version 1. In: Boulder, C.U. (Ed.), National Snow and Ice Data Center. DOI:https://doi.org/10.7265/N5TB14TC

Noor, K. et al., 2023. Snow sampling strategy can bias estimation of meltwater fractions in isotope hydrograph separation. Journal of Hydrology, 627: 130429. DOI:https://doi.org/10.1016/j.jhydrol.2023.130429

Pelletier, A., Andréassian, V., 2020. Hydrograph separation: an impartial parametrisation for an imperfect method. Hydrol. Earth Syst. Sci., 24(3): 1171-1187. DOI:10.5194/hess-24-1171-2020

Piggott, A.R., Moin, S., Southam, C., 2005. A revised approach to the UKIH method for the calculation of baseflow / Une approche améliorée de la méthode de l'UKIH pour le calcul de l'écoulement de base. Hydrological Sciences Journal, 50(5): null-920. DOI:10.1623/hysj.2005.50.5.911

Price, K., 2011. Effects of watershed topography, soils, land use, and climate on baseflow hydrology in humid regions: A review. Progress in Physical Geography: Earth and Environment, 35(4): 465-492. DOI:10.1177/0309133311402714

Rudin, C., 2019. Stop Explaining Black Box Machine Learning Models for High Stakes Decisions and Use Interpretable Models Instead. Nat Mach Intell, 1(5): 206-215. DOI:10.1038/s42256-019-0048-x

https://doi.org/10.5194/egusphere-2025-6011
Preprint. Discussion started: 12 December 2025


Sheta, A., Abdel-raouf, A., Fraihat, K., Baareh, A.K., 2023. Evolutionary Design of a PSO-Tuned Multigene Symbolic Regression Genetic Programming Model for River Flow Forecasting. International Journal of Advanced Computer Science and Applications, 14: 2023. DOI:10.14569/IJACSA.2023.0140489

Song, W. et al., 2024. Towards data-driven discovery of governing equations in geosciences. Communications Earth & Environment, 5(1): 589. DOI:10.1038/s43247-024-01760-6

Stewart, M.K., 2015. Promising new baseflow separation and recession analysis methods applied to streamflow at Glendhu Catchment, New Zealand. Hydrol. Earth Syst. Sci., 19(6): 2587-2603. DOI:10.5194/hess-19-2587-2015

Stoelzle, M., Schuetz, T., Weiler, M., Stahl, K., Tallaksen, L.M., 2020. Beyond binary baseflow separation: a delayed-flow index for multiple streamflow contributions. Hydrology and Earth System Sciences, 24(2): 849-867. DOI:10.5194/hess-24-849-2020

Tan, X., Liu, B., Tan, X., 2020. Global Changes in Baseflow Under the Impacts of Changing Climate and Vegetation. Water Resources Research, 56(9): e2020WR027349. DOI:https://doi.org/10.1029/2020WR027349

Tarasova, L., Gnann, S., Yang, S., Hartmann, A., Wagener, T., 2024. Catchment characterization: Current descriptors, knowledge gaps and future opportunities. Earth-Science Reviews, 252. DOI:10.1016/j.earscirev.2024.104739

Thorslund, J., van Vliet, M.T.H., 2020. A global dataset of surface water and groundwater salinity measurements from 1980–2019. Scientific Data, 7(1): 231. DOI:10.1038/s41597-020-0562-z

Wang, C., Gomez-Velez, J.D., Wilson, J.L., 2022. Dynamic coevolution of baseflow and multiscale groundwater flow system during prolonged droughts. Journal of Hydrology, 609. DOI:10.1016/j.jhydrol.2022.127657

Wilstrup, C., Kasak, J., 2021. Symbolic regression outperforms other models for small data sets. arXiv preprint arXiv:2103.15147.

Wu, S., Zhao, J., Wang, H., Sivapalan, M., 2021. Regional Patterns and Physical Controls of Streamflow Generation Across the Conterminous United States. Water Resources Research, 57(6). DOI:10.1029/2020wr028086

Xie, J. et al., 2024. Majority of global river flow sustained by groundwater. Nature Geoscience. DOI:10.1038/s41561-024-01483-5

Xie, J. et al., 2022. Estimating Gridded Monthly Baseflow From 1981 to 2020 for the Contiguous US Using Long Short‐Term Memory (LSTM) Networks. Water Resources Research, 58(8). DOI:10.1029/2021wr031663

Xie, J. et al., 2020. Evaluation of typical methods for baseflow separation in the contiguous United States. Journal of Hydrology, 583. DOI:10.1016/j.jhydrol.2020.124628

Yan, X. et al., 2023. Detecting and attributing the changes in baseflow in China's Loess Plateau. Journal of Hydrology, 617: 128957. DOI:https://doi.org/10.1016/j.jhydrol.2022.128957

Zhang, J., Zhang, Y., Song, J., Cheng, L., 2017. Evaluating relative merits of four baseflow separation methods in Eastern Australia. Journal of Hydrology, 549: 252-263. DOI:10.1016/j.jhydrol.2017.04.004

Zhang, J. et al., 2020. Large-scale baseflow index prediction using hydrological modelling, linear and multilevel regression approaches. Journal of Hydrology, 585: 124780. DOI:https://doi.org/10.1016/j.jhydrol.2020.124780